Available online at www.sciencedirect.com
ScienceDirect
Applied Mathematical Modelling 31 (2007) 1308–1320
APPLIED MATHEMATICAL MODELLING
www.elsevier.com/locate/apm

Modelling a copper electrowinning cell based on reactive electrodialysis

L. Cifuentes [a,*], J.M. Castro [a], G. Crisóstomo [a], J.M. Casas [b], J. Simpson [c]

[a] Departamento de Ingeniería de Minas, Universidad de Chile, Tupper 2069, Santiago, Chile
[b] Departamento de Ingeniería, Química y Biotecnología, Universidad de Chile, Beauchef 861, Santiago, Chile
[c] Departamento de Ingeniería Metalúrgica, Universidad de Santiago, Ecuador 3659, Santiago, Chile

Received 1 December 2004; received in revised form 1 December 2005; accepted 20 February 2006
Available online 10 July 2006

Abstract

This work reports the development of a mathematical model for the operation of a laboratory-scale copper electrowinning cell based on reactive electrodialysis (RED). Data were obtained from experiments and from the literature. The cathodic reaction was copper electrodeposition and the anodic reaction was ferrous to ferric ion oxidation. The catholyte was aqueous cupric sulphate in sulphuric acid and the anolyte was aqueous ferrous sulphate in sulphuric acid. An anion membrane separated anolyte from catholyte while keeping a conductive path between them. The model includes (a) the cathodic and anodic kinetics, (b) the speciation of catholyte and anolyte and (c) ion transport through the membrane. The computer code was implemented in MATLAB software. The model was calibrated and validated and its predictions are in good agreement with experimental results for: amount of deposited copper, amount of produced Fe(III) species, cell voltage and specific energy consumption.

Keywords: Modelling; Copper; Electrowinning cell; Reactive electrodialysis

1. Introduction

1.1. Limitations of conventional copper electrowinning cells

The operation of conventional copper electrowinning cells is limited by three main factors [1–3]: (a) Low mass transfer rates due to a low electrolyte flowrate. (b) Low specific surface area (m^2/kg) of the cathodes, due to the fact that sheet cathodes offer little surface area per unit weight to the reaction. (c) High energy requirements (about 2 kW h per kg of produced copper), which is a result of an anodic reaction ($2H_2O \rightarrow O_2 + 4H^+ + 4e$), which takes place on lead anodes. The standard equilibrium potential for this

* Corresponding author. Tel.: +562 2695684; fax: +562 6723504.
E-mail address: luicifue@ing.uchile.cl (L. Cifuentes).

0307-904X/$ - see front matter © 2006 Elsevier Inc. All rights reserved.
doi:10.1016/j.apm.2006.02.016

Nomenclature

a anodic subindex
a, s anodic subindex for a secondary reaction
A surface area perpendicular to ion migration path, m^2
A_a, A_c, A_m surface area of anode, cathode and membrane, m^2
A_γ Debye-Hückel parameter, $kg^{0.5}\,mol^{-0.5}$
B_γ Debye-Hückel parameter, $kg^{0.5}\,mol^{-0.5}\,Å^{-1}$
$\dot{B}$ B-dot parameter, $kg\,mol^{-1}$
c cathodic subindex
c, s cathodic subindex for a secondary reaction
C, C^{2+}_{Cu}, C^{2+}_{Fe} concentration of ionic species, $mol\,L^{-1}$
C_{tot} total concentration of charged species in anolyte, $mol\,L^{-1}$
$\overline{C}_{sulphate}$ average sulphate concentration (anolyte and catholyte), $mol\,L^{-1}$
d length of ion migration path, m
D diffusivity, $m^2\,s^{-1}$
D_{ef} effective diffusivity, $m^2\,s^{-1}$
D_{H^+} diffusivity of H^+, $m^2\,s^{-1}$
$E_{e,a}$ equilibrium potential, main anodic reaction, V
$E_{e,c}$ equilibrium potential, main cathodic reaction, V
F Faraday constant, $C\,eq^{-1}$
G gas constant, $J\,mol^{-1}\,K^{-1}$
i, i_a, i_c current density, anodic and cathodic, $A\,m^{-2}$
i_L, $i_{L,a}$, $i_{L,c}$ limiting current density, anodic and cathodic, $A\,m^{-2}$
i^b_0, $i^b_{0,a}$, $i^b_{0,c}$ exchange current density, anodic and cathodic reactions, in terms of reactant concentrations in the bulk solution, $A\,m^{-2}$
$i'^{\,b}_0$ modified exchange current density, $A\,m^{-2}\,L\,mol^{-1}$
i^{sf}_0 exchange current density in terms of reactant concentrations at the electrode surface, $A\,m^{-2}$
I cell current, A
I_γ ionic strength, $mol\,kg^{-1}$
j species subindex
k, k_a, k_c mass transfer coefficient, anodic and cathodic, $m\,s^{-1}$
K^0_f equilibrium constant of formation
m membrane subindex
$m_{Cu,\,dep}$ experimentally determined deposited copper mass, kg
$m_{Cu,\,calc}$ deposited copper mass calculated by Faraday's law, kg
N ionic flux, $mol\,m^{-2}\,s^{-1}$
N_{dif} diffusion flux, $mol\,m^{-2}\,s^{-1}$
N_{mig} migration flux, $mol\,m^{-2}\,s^{-1}$
n amount of H^+ transported through the membrane, moles
r ionic radius, m
R_a, R_c, R_m electrical resistance of anolyte, catholyte and membrane, Ω
t time of operation, s
T temperature, K
V_a anolyte volume, m^3
V_{cell} cell voltage, V
x membrane thickness, m
z, z_a, z_c charge number, anodic and cathodic reactions
$z_{sulphate}$ sulphate charge number
α_a, α_c anodic and cathodic charge transfer coefficients

γ	activity coefficient
ΔE_e	difference between the equilibrium potentials of the main reactions, V
κ	electrical conductivity, $\Omega^{-1}\,m^{-1}$
η, η_a, η_c	overpotential, anodic and cathodic, V
η_{curr}	current efficiency, %
Φ	inner or Galvani potential, V

reaction is 0.89 V higher than the corresponding value for the cathodic reaction ($Cu^{2+} + 2e \rightarrow Cu^0$); it also exhibits an anodic overpotential close to 0.8 V. Additionally, this reaction produces 'acid mist' (air contamination with sulphuric acid) in industrial plants.

To increase the cell current density it would be advantageous to use reactor designs which allowed electrolyte agitation and cathodes of high specific surface area, e.g. particulate, porous or mesh cathodes. It would also be convenient to use a less energy-intensive anodic reaction and a more catalytic anode material to reduce the cell voltage and the energy cost of the operation.

1.2. New electrowinning cell designs

Various cell designs have been studied during the last 20 years [1,4,5], the best known of which are the fluidized bed cell [6,7] and the spouted bed cell [4,5,8], however, few industrial implementations of non-conventional copper electrowinning cells are known.

Several alternative anodic reactions have also been studied [2,9]. On cost and environmental grounds, the one which appears most promising is the ferrous to ferric ion oxidation ($Fe^{2+} \rightarrow Fe^{3+} + e$) [9,10]. One way of using this reaction, while avoiding the deleterious effect of the ferric ion on cathodic efficiency, consists of using two electrolytes (anolyte and catholyte) instead of one, while conserving a conductive path between them. This is possible by using an electrodialytic membrane to separate species and to obtain specific reactions at one or both electrodes. This process is known as reactive electrodialysis [11,12]. The study of these systems requires a detailed knowledge of the speciation of the electrolytes, i.e., the determination of the species present and their concentrations as functions of pH, temperature and the abundance of key system components [13]. The application of electrodialysis to copper electrometallurgy, as well as the thermodynamic modelling of the speciation of the related electrolytes, are recent developments [12–15].

A lab-scale cell which implements a reactive electrodialysis design with mesh electrodes, agitated electrolytes and ferrous to ferric ion oxidation as anodic reaction on various anode materials, has recently been developed [11,12].

1.3. Electrowinning cell models

Mathematical models of electrochemical cells have been proposed by a number of authors. Modelling principles, including formulation of equations and numerical methods for their solution, have been published for fluid mechanics, heat transfer, chemical kinetics and transport processes [16]. Several authors have also included the electrode kinetics [16–19]. Models for conventional electrowinning cells have been produced [20].

2. Experimental methodology

2.1. Reactive electrodialysis (RED) cell

Experiments were carried out in a lab-scale copper electrowinning cell based on reactive electrodialysis (Fig. 1). The cell is made of acrylic and it consists of two compartments. The first one contains anode and anolyte and the second one, cathode and catholyte. Both electrolytes were recirculated to separate 1 L tanks

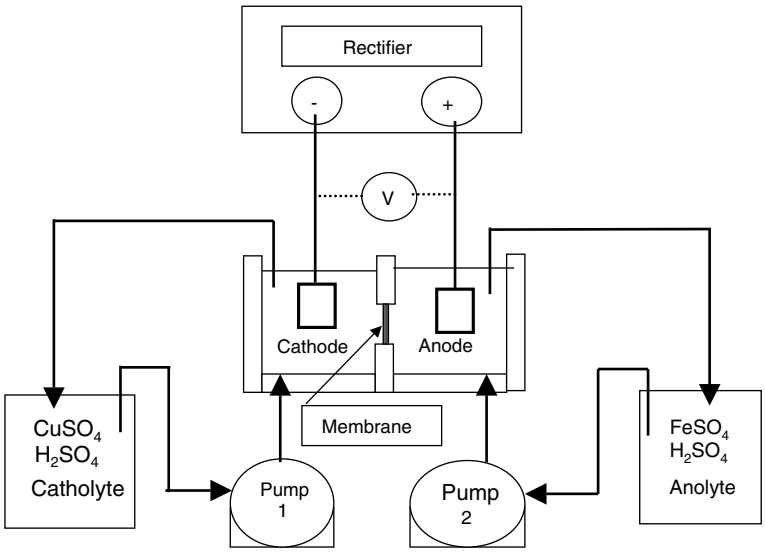

Fig. 1. Experimental set up, showing RED cell, rectifier and recirculation tanks.

by means of Watson–Marlow 505 S peristaltic pumps at a flow rate of 900 cm^3/min. The effective volume of catholyte and anolyte in the compartments was 275 cm^3 each, while their total volume was 450 cm^3 each.

The cathode was a 4 cm^2 copper sheet (its back face masked with Teflon tape) and the anode was a 4 cm^2 platinum sheet, equally masked. An Ionac MA3475 anion membrane, whose aim was to hinder the passage of cations between the electrolytes, was placed in a 2 cm by 2 cm window cut in the acrylic plates between the compartments. The membrane was kept in place by two 2 mm thick rubber seals. The anolyte composition was 190 g/L H_2SO_4 and 28 g/L Fe(II) (as $FeSO_4 \cdot 7H_2O$). The catholyte composition was 190 g/L H_2SO_4 and 40 g/L Cu(II) (as $CuSO_4 \cdot 5H_2O$). The cell was operated at 50 ± 1 °C. The temperature was kept constant by a Julabo thermostatic bath. The conditions described here were applied to all the experiments reported in this work.

2.2. Electrochemical kinetics

Potentiodynamic experiments were carried out in the RED cell with a Solartron 1286 electrochemical interface in order to determine the anodic and cathodic kinetics on the studied electrodes and electrolytes. A mercury/mercury sulphate reference electrode with Luggin capillary was used ($E^0_{50\,^\circ C} = 0.645$ V against SHE). For the cathodic sweep, the working electrode was copper sheet and the counterelectrode was platinum sheet; for the anodic sweep, the working electrode was platinum sheet and the counterelectrode was copper sheet. The sweep rate was 1.0 mV/s.

2.3. Electrical conductivity

The electrical conductivity of anolyte and catholyte was measured with a Jenco 1671 conductivity unit.

2.4. Limiting current density for transport through the membrane

An experiment was carried out in the RED cell in order to establish the value of the limiting current density for ion transport through the membrane. The cell current was increased in 80 mA steps and the cell voltage was continuously monitored. After each current increase, it was waited until the cell voltage reached a constant value and then its value was recorded. The test finished when the cell current came close to the rectifier's upper current limit (2 A).

2.5. RED cell validation run

In order to validate the model, a 4 h run was carried out in the above described RED cell in order to determine the dependence on time of: (a) the cell voltage; (b) Cu(II) concentration in the catholyte and (c) Fe(II) and Fe(III) concentrations in the anolyte. The cell was operated with a cell current density of 400 A/m^2 provided by a 2 A, 30 V rectifier. The cell voltage was continuously monitored. Copper and iron were analyzed by atomic absorption spectroscopy. The deposited copper mass was also measured.

3. Modelling

The developed model describes and quantifies the anodic and cathodic electrode kinetics, ion transport through the membrane and the speciation for the Cu(II)–H_2SO_4–H_2O catholyte and the Fe(II)–Fe(III)–H_2SO_4–H_2O anolyte.

3.1. Electrolyte speciation

Tables 1 and 2 present the components, species and main chemical reactions at 50 °C for catholyte and anolyte.

The speciation model consists of a set of equations for the mass balances of the system's components and the equilibrium relationships for all the species present in the studied systems [13]. The activity for each species is obtained from the equilibrium constants (K_f^0) and activity coefficients (γ) calculated by an extended Debye–Hückel equation:

$$\log \gamma_j = -\frac{A_\gamma z_j^2 \sqrt{I_\gamma}}{1 + r_j B_\gamma \sqrt{I_\gamma}} + \dot{B} \cdot I_\gamma. \tag{1}$$

Mass balance equations for anolyte and catholyte in the studied systems have been published elsewhere [13,21].

Table 1
Speciation model for the anolyte: Fe(II)–Fe(III)–H_2SO_4–H_2O

Species	Components				$\log K_f^0$ (50°)
	H^+	SO_4^{2-}	Fe^{2+}	Fe^{3+}	
HSO_4^-	1	1	0	0	2.32
$FeHSO_4^+$	1	1	1	0	1.90
$FeSO_{4(aq)}$	0	1	1	0	2.44
$FeHSO_4^{2+}$	1	1	0	1	3.48
$FeH(SO_4)_{2(aq)}$	1	2	0	1	10.2
$Fe(SO_4)_2^-$	0	2	0	1	7.64
$FeSO_4^+$	0	1	0	1	4.76
Molality	1–5	0.5–2.5	0–1	0–1	

Table 2
Speciation model for the catholyte: Cu–H_2SO_4–H_2O

Species	Components			$\log K_f^0$ (50°)
	H^+	SO_4^{2-}	Cu^{2+}	
HSO_4^-	1	1	0	2.32
$CuSO_{4(a)}$	0	1	1	2.61
Molality	1–5	0.5–2.5	0–1	

3.2. Electrode kinetics

Possible electrode reactions are:

$$\text{At the anode:} \quad Fe^{2+} \rightarrow Fe^{3+} + e \quad \text{(main reaction)} \tag{2}$$

$$2H_2O \rightarrow O_2 + 4H^+ + 4e \quad \text{(secondary reaction)} \tag{3}$$

$$\text{At the cathode:} \quad Cu^{2+} + 2e \rightarrow Cu^0 \quad \text{(main reaction)} \tag{4}$$

$$2H^+ + 2e \rightarrow H_2 \quad \text{(secondary reaction)} \tag{5}$$

If an undesired transport of ferric ions through the anion membrane takes place, then the additional cathodic reaction:

$$Fe^{3+} + e \rightarrow Fe^{2+} \tag{6}$$

could reduce the cathodic current efficiency.

For the main reactions, the current densities are calculated by expressions for mixed control derived from Butler–Volmer and Fick equations [22]. For the cathodic reaction:

$$|i_c| = \frac{i_{0c}^b |i_{Lc}|}{i_{0c}^b + |i_{Lc}| \exp\left(\frac{\alpha_c F}{GT}\eta_c\right)} \tag{7}$$

and for the anodic reaction:

$$i_a = \frac{i_{0a}^b i_{La}}{i_{0a}^b + i_{La} \exp\left(\frac{-\alpha_a F}{GT}\eta_a\right)}. \tag{8}$$

Taking into account that the exchange current density may be expressed as

$$i_0^b = i_0'^b C, \tag{9}$$

where C is the bulk concentration of the reacting species, and given that the limiting current density is given by

$$i_L = zFkC, \tag{10}$$

then the expression for the cathodic reaction rate with explicit reactant concentrations is

$$|i_c| = \frac{i_{0c}'^b C_{Cu^{2+}}^2 z_c F k_c}{i_{0c}'^b\ C_{Cu^{2+}} + z_c F k_c C_{Cu^{2+}} \exp\left(\frac{\alpha_c F}{GT}\eta_c\right)} \tag{11}$$

and for the anodic reaction:

$$i_a = \frac{i_{0a}'^b C_{Fe^{2+}}^2 z_a F k_a}{i_{0a}'^b C_{Fe^{2+}} + z_a F k_a C_{Fe^{2+}} \exp\left(\frac{-\alpha_a F}{GT}\eta_a\right)}. \tag{12}$$

For secondary reactions, i.e., hydrogen ion reduction to gaseous hydrogen at the cathode and water oxidation to gaseous oxygen at the anode, high-field approximations to the Butler–Volmer equation were used to calculate the reaction rates, as they are controlled by charge transfer in the studied potential range.

$$i_{a,s} = i_{0,a,s}^{sf} \exp\left(\frac{\alpha_{a,s} F}{GT}\eta_{a,s}\right), \tag{13}$$

$$|i_{c,s}| = i_{0,c,s}^{sf} \exp\left(\frac{-\alpha_{c,s} F}{GT}\eta_{c,s}\right). \tag{14}$$

The cell voltage is:

$$V_{cell} = \Delta E_e + \eta_a + |\eta_c| + I(R_a + R_c + R_m), \tag{15}$$

where $\Delta E_e = E_{e,a} - E_{e,c}$.

The electrical resistances of anolyte and catholyte are given by

$$R = \frac{1}{\kappa}\frac{d}{A}. \tag{16}$$

The method used to determine the membrane resistance is given in the following section.

3.3. Transport phenomena

Taking into account migration and diffusion phenomena, the transport flux through the membrane in dilute solutions is given by

$$N_{j,\mathrm{m}} = N_{\mathrm{mig}} + N_{\mathrm{dif}} = -\frac{z_j F}{GT} D_j C_{j,\mathrm{m}} \frac{\partial \Phi}{\partial x} - D_j \nabla C_j. \tag{17}$$

For concentrated solutions, the transport flux is given by the same expression, but the diffusivities are replaced by 'effective diffusivities' (D_{ef}), which are experimentally determined (see Section 3.6).

Ohm's law provides a relationship between current density and potential gradient:

$$i = -\kappa \nabla \Phi \tag{18}$$

and the electroneutrality condition is

$$\sum C_j z_j = 0. \tag{19}$$

The electrical conductivity of dilute electrolytes is given by

$$\kappa = \frac{F^2}{GT} \sum z_j^2 C_j D_j. \tag{20}$$

As in Eq. (17) above, for concentrated electrolytes the diffusivities are replaced by 'effective diffusivities'.

Faraday's law links current density to ion flux as

$$i = F \sum z_j N_j. \tag{21}$$

The membrane resistance (R_{m}) was calculated from a mass balance of charged species in anolyte and catholyte assuming: (a) electroneutrality in both electrolytes and (b) that H^+ transports through the membrane only by diffusion whereas sulphate transports only by migration [23,24]. The resulting expression is

$$R_{\mathrm{m}} = \frac{GTV_{\mathrm{a}} x \left(C_{\mathrm{tot}} - \frac{n}{V_{\mathrm{a}}} \right)}{IFA_{\mathrm{m}} t 2 D_{\mathrm{H}^+} z_{\mathrm{sulphate}} \overline{C}_{\mathrm{sulphate}}}. \tag{22}$$

3.4. Algorithm

The implemented algorithm begins with data input and then defines a time step which determines the number of iterations to be carried out for a given cell operation time. For each iteration, the following calculations are performed: (a) speciation of anolyte and catholyte; (b) transport of ionic species through the membrane; (c) electrical conductivity of anolyte and catholyte; (d) anodic and cathodic overpotentials; (e) equilibrium potentials for electrode reactions; (f) cell voltage; (g) deposited copper mass; (h) produced amount of Fe(III) species; (i) mass balances for anolyte and catholyte. Then, the time of operation is incremented by a time step (5 min) and the calculations are performed once again, taking into account the changes in the concentrations of reactants caused by the electrode reactions. The process is repeated until the total operation time is reached.

3.5. Model solution

The speciation model consists of a set of non-linear equations. It is solved by an iterative algorithm which implements a Newton–Raphson method for a multi-dimensional system. Results from the speciation model are fed into a dynamic model of cell operation, which includes calculations for both the electrode kinetics

and the mass transport across the membrane. Both models were coded using MATLAB software on a personal computer. Kinetic parameters were determined from experimental data; mixed control Eqs. (7 and 8) were fitted to data for the main reactions (2 and 4) and high-field approximations to the Butler–Volmer Eqs. (13 and 14) were fitted to data for secondary reactions (3 and 5). Other data (effective diffusivities, Debye–Hückel parameters and electrical conductivities of solutions) are presented in Tables 3a and 3b. Further data for the speciation model have been published elsewhere [25].

3.6. Model calibration

'Effective diffusivities', i.e., diffusivities of species in concentrated electrolytes were obtained from experimentally determined electrical conductivity values (see Section 2) according to a procedure proposed by Casas et al. [13,15,26]. The measured conductivities are in Table 3b. The obtained 'effective diffusivities' (D_{ef}, Table 3a) allowed the use of Eq. (17) for the concentrated electrolytes used in this work. They also allowed the use of Eq. (20) for the calculation of electrical conductivities at any given concentration of the relevant solution components. Diffusivities in the membrane (Table 3a) were estimated from published data [23,24].

The kinetic parameters for all the relevant electrochemical reactions were obtained from experiments as explained above. The potentiodynamic sweeps produced the parameters shown in Table 4. Fig. 2 shows the

Table 3a
Model data at 50 °C – effective diffusivities

Effective diffusivities in solution[a], $m^2\ s^{-1} \times 10^8$	
Catholyte	
H^+	0.295
SO_4^{2-}	0.664
Cu^{2+}	0.443
HSO_4^-	0.664
$CuHSO_4^+$	0.664
Anolyte	
H^+	0.278
SO_4^{2-}	0.626
Fe^{2+}	0.417
Fe^{3+}	0.278
HSO_4^-	0.626
$FeHSO_4^+$	0.626
$FeHSO_4^{2+}$	0.626
$Fe(SO_4)_2^-$	0.626
$FeSO_4^+$	0.626
Diffusivities in the membrane[b], $m^2\ s^{-1}$	
H^+	2.4×10^{-6}
SO_4^{2-}	4.5×10^{-8}

[a] Calculated from conductivity measurements.
[b] Estimated from published data [23,24].

Table 3b
Other model data at 50 °C

Debye–Hückel parameters for the electrolytes[a]	
A_γ, $kg^{0.5}\ mol^{-0.5}$	0.5365
B_γ, $kg^{0.5}\ mol^{-0.5}\ Å^{-1}$	0.3329
$\dot{B}$, $kg\ mol^{-1}$	0.0430
Electrical conductivities of electrolytes[b], $\Omega^{-1}\ m^{-1}$	
Anolyte	76.5
Catholyte	73.9

[a] Estimated from published data [13,25].
[b] Measured.

Table 4
Kinetic parameters for cathodic and anodic reactions at 50 °C (determined by experiment)

Reaction	i_0, A/m^2	α	i_L, A/m^2
Cu^{2+}/Cu^0	36.0	0.46	1211
H^+/H_2	4.1	0.24	–
Fe^{2+}/Fe^{3+}	53.0	0.64	735
H_2O/O_2	0.023	0.17	–

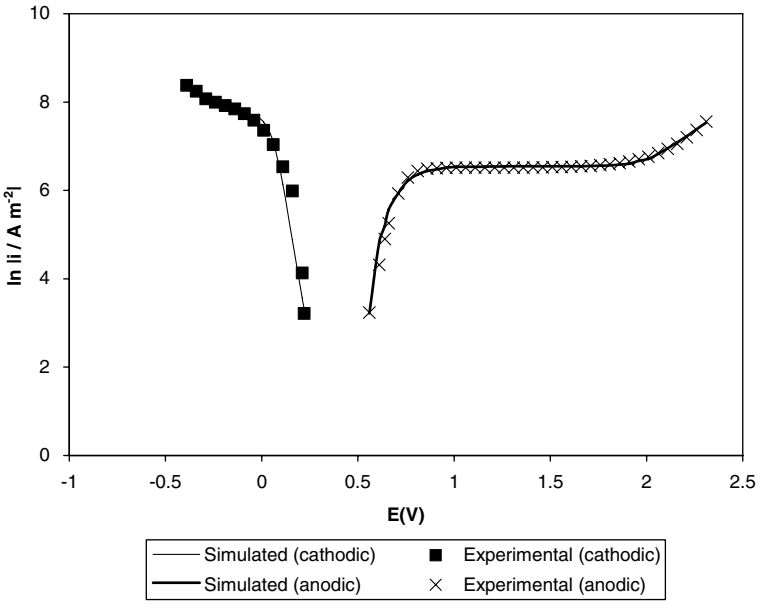

Fig. 2. Evans diagram showing experimental results and fitted curves for potentiodynamic sweeps. Cathodic reactions are copper deposition and hydrogen evolution. Anodic reactions are Fe(II) oxidation and oxygen evolution.

result of the curve fitting procedure. The hydrogen reduction and water oxidation reactions do not exhibit limiting current densities in the studied potential ranges, because of the very high concentrations of the reactants (protons and water) in the studied solutions.

3.7. Model validation

Model validation was achieved by carrying out an ad hoc experiment in the RED cell and comparing the results with the corresponding model calculations. The test variables were copper production rate, Fe(III) production rate, cell voltage and specific energy consumption. The operation parameters for the cell during the validation experiment are in Table 5.

Table 5
Operation parameters for the EW-RED cell

Parameters	Values
Cell current density	400 A/m^2
Anolyte composition	190 g/L H_2SO_4; 28.0 g/L (as $FeSO_4 \cdot 7H_2O$)
Catholyte composition	190 g/L H_2SO_4; 40.0 g/L Cu(II) (as $CuSO_4 \cdot 5H_2O$)
Electrolyte temperature	50 °C
Electrolyte flow rate	900 cm^3/min
Anode material	Platinum sheet
Cathode material	Copper sheet
Interelectrode distance	10 mm
Surface area	$A_m = A_a = A_c = 0.0004$ m^2

4. Results and discussion

4.1. Speciation of anolyte and catholyte

Results for the speciation of anolyte and catholyte at 25 °C and 50 °C are presented in Table 6. Both electrolytes exhibit high ionic strengths (about 3.2 molal) and high association degrees between metallic ions and sulphate.

The main species predicted by the speciation model in the anolyte were HSO_4^-, H^+, Fe^{2+}, $FeSO_{4(aq)}$ and $FeH(SO_4)_{(aq)}$, and in the catholyte, they were HSO_4^-, H^+, $CuSO_{4(aq)}$ and Cu^{2+}. The concentrations of Fe^{3+} and free SO_4^{2-} were very low due to their tendency to associate as iron (III) sulphate. The concentrations of H^+, HSO_4^-, Fe^{2+} and Cu^{2+} were high, indicating that these species were stable in studied conditions.

4.2. Limiting current density for transport through the membrane

For the experimental run designed to determine the limiting current density for ion transport through the membrane, the final cell current density was 4700 A/m^2, which represents the upper limit for the power source. Up to that value no limitation was apparent. This means that the limiting current density originated by the

Table 6
Aqueous speciation for anolyte and catholyte at 25 and 50 °C

Species	Concentration (mol/kg)	
	25 °C	50 °C
Anolyte[a]		
H^+	1.79	1.71
SO_4^{2-}	9.44×10^{-2}	4.91×10^{-2}
Fe^{2+}	3.70×10^{-1}	3.62×10^{-1}
Fe^{3+}	8.19×10^{-7}	6.11×10^{-8}
HSO_4^-	2.36	2.40
$FeHSO_4^+$	2.30×10^{-2}	6.50×10^{-2}
$FeSO_4^0$	1.07×10^{-1}	7.33×10^{-2}
$FeHSO_4^{2+}$	1.39×10^{-5}	4.91×10^{-6}
$Fe(SO_4)_2^-$	6.71×10^{-5}	2.19×10^{-4}
$FeSO_4^+$	4.56×10^{-5}	8.40×10^{-6}
$FeH(SO_4)_2^0$	9.87×10^{-3}	9.77×10^{-3}
Ionic strength	3.01	2.91
Catholyte[b]		
H^+	1.73	1.65
SO_4^{2-}	1.02×10^{-1}	5.37×10^{-2}
Cu^{2+}	4.66×10^{-1}	4.93×10^{-1}
HSO_4^-	2.45	2.53
$CuSO_4^0$	1.84×10^{-1}	1.57×10^{-1}
Ionic strength	3.23	3.18

[a] Anolyte composition: $[H_2SO_4] = 2.09$ m; $[Fe(II)] = 0.5$ m; $[Fe(III)] = 0.01$ m.
[b] Catholyte composition: $[H_2SO_4] = 2.09$ m; $[Cu(II)] = 0.65$ m.

Table 7
Experimental and simulated results for the operation of a copper electrowinning cell based on reactive electrodialysis[a]

Variable	Unit	Experimental value	Simulated value	Relative error (%)
Copper production	kg/h	1.85×10^{-4}	1.90×10^{-4}	2.7
Fe(III) production	kg/h	3.27×10^{-4}	3.30×10^{-4}	0.9
Average cell voltage	V	0.893	0.895	0.2
Energy consumption	kW h/kg Cu	0.771	0.795	3.1

[a] Cell operation parameters are shown in Table 1.

membrane is higher than 4700 A/m^2. As the cell was run at 400 A/m^2, mass transfer through the membrane did not limit the operation of the RED cell.

4.3. Model validation

A comparison between experiment and model prediction for the test variables is given in Table 7 and discussed in the following paragraphs.

4.4. Cell voltage

The variation of the cell voltage with time, for a cell current density of 400 A/m^2 in a 4 h run, is given in Fig. 3. Initially, the model overestimates the cell voltage by about 13%, but after 5 min (cell operation time), the predicted value coincides with the measured value. From then on, the simulated and experimental values are practically the same, with a relative error of 0.2% for the predicted average cell voltage.

The cell voltage is made up of the following components: (a) difference between the equilibrium potentials of the main reactions, 23%; (b) anodic overpotential, 32%; (c) cathodic overpotential, 28%; (d) potential drop in the anolyte, 3%; (e) potential drop in the catholyte, 4%; (f) potential drop in the membrane, 10%.

4.5. Copper production

The measured amount of deposited copper for a 4 h run was 7.4×10^{-4} kg and the theoretical mass, calculated with Faraday's law, was 7.6×10^{-4} kg.

The cathodic current efficiency (η_{curr}), calculated as

$$\eta_{curr} = \frac{m_{Cu,dep}}{m_{Cu,calc}} \cdot 100 \tag{23}$$

was 97.4%.

Fig. 4 shows the dependence on time of the concentration of copper species in the catholyte and of the mass of deposited copper, as predicted by the model. As copper is deposited on the cathode, the concentration of copper-containing species decreases with time.

4.6. Production of ferric species

Fig. 5 shows the dependence on time of the concentration of Fe(II) and Fe(III) species. As Fe(II) species are continuously oxidized at the anode, the concentration of Fe(III) species in the anolyte increases with time, whereas the concentration of Fe (II) species decreases.

The rate of production of Fe(III) species predicted by the model was 3.27×10^{-4} kg/h, whereas the experimental value was 3.30×10^{-4} kg/h (Table 7). The error is 0.9%.

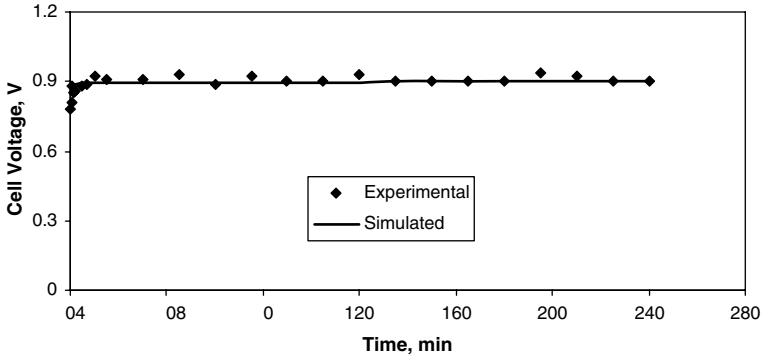

Fig. 3. Measured and simulated cell voltage versus time of cell operation.

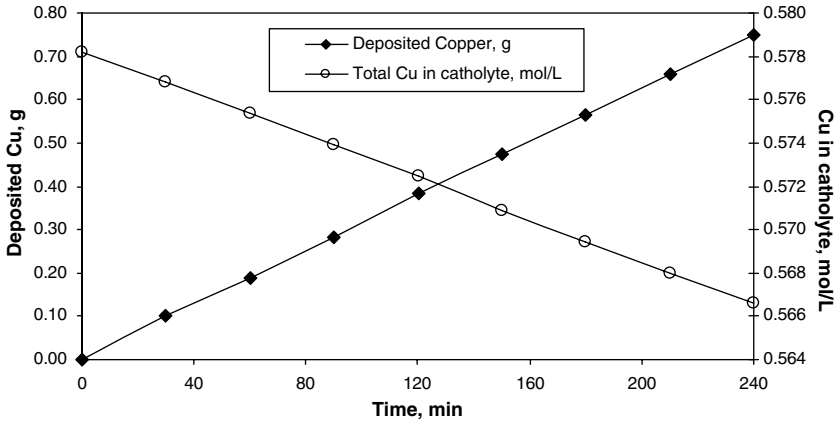

Fig. 4. Mass of deposited copper and copper concentration in the catholyte versus time of cell operation (simulated results).

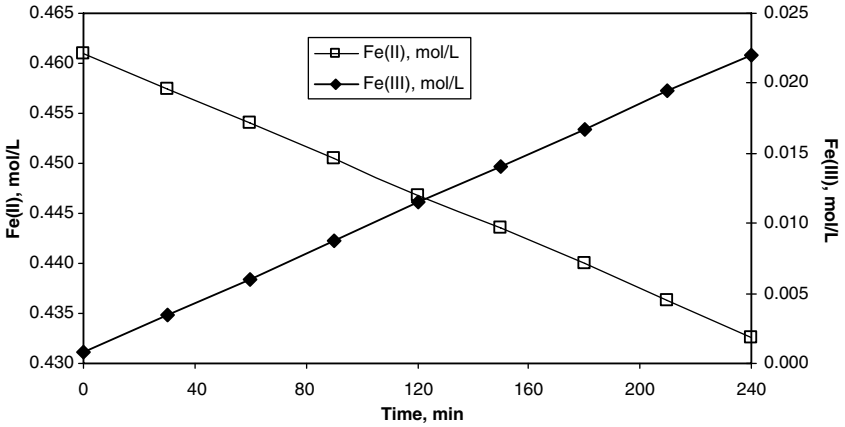

Fig. 5. Fe(II) and Fe(III) concentrations in the anolyte versus time of cell operation (simulated results).

4.7. Specific energy consumption

Table 7 shows that the difference between calculation and experiment for specific energy consumption is about 3.1%, which confirms the good agreement exhibited by previous results.

5. Conclusions

(1) In the studied conditions, it is possible to simulate the behaviour of a lab-scale copper electrowinning cell based on reactive electrodialysis using a dynamic (time-dependent) mathematical model which includes the cathodic and anodic electrochemical kinetics, the speciation of catholyte and anolyte and ion transport through the membrane.
(2) Agreement between experiment and model prediction is good (between 0.2% and 3.1% error) for copper production rate, Fe(III) production rate, cell voltage and specific energy consumption.
(3) The developed model could be useful to assist in the design and operation of copper electrowinning cells based on reactive electrodialysis.
(4) The model can be enhanced by allowing for variations in temperature, recirculation flowrate and cell geometry.

Acknowledgement

This work was funded by the National Committee for Science and Technology (CONICYT, Chile) via FONDECYT project No. 101 0138. Financial support from Placer Dome to the Chair of Environmental Studies in Mining, as well as the continued support from the Departments of Mining Engineering and Chemical Engineering and Biotechnology, Universidad de Chile, are gratefully acknowledged.

References

[1] R. Kammel, Metal recovery from dilute aqueous solutions by various electrochemical reactors, in: R. Bautista (Ed.), Hydrometallurgical Process Fundamentals, Elsevier Science, Amsterdam, Netherlands, 1982, pp. 617–648.
[2] W.C. Cooper, Advances and future prospects in copper electrowinning, J. Appl. Electrochem. 15 (1985) 789–805.
[3] C.K. Gupta, T.K. Mukherjee, Hydrometallurgy in Extraction Processes, CRC Press, Boca Raton, USA, 1990.
[4] S. Siu, J.W. Evans, Spouted bed electrowinning of copper, in: W.C. Cooper (Ed.), Proceedings of the COPPER '95 International Conference, vol. 3, The Metallurgical Society of CIM, Toronto, Canada, 1995.
[5] V. Jiricny, A. Roy, J.W. Evans, A study of the spouted-bed electrowinning of copper, in: J. Dutrizac (Ed.), Proceedings of the COPPER'99 International Conference, vol. 3, TMS, Warrendale, USA, 1999, pp. 629–642.
[6] F. Goodridge et al., Copper deposition in a pilot plant scale fluidized bed, Electrochim. Acta 24 (1979) 1237–1242.
[7] F. Masterson et al., Fluidized bed EW of Cu: experiments using 150 A cells and some mathematical modelling, Met. Trans. B 13B (1982) 3–13.
[8] V.D. Stankovic, S. Stankovic, An investigation of the spouted bed electrode cell for the EW of metals from dilute solutions, J. Appl. Electrochem. 21 (1991) 124–129.
[9] A.V. Cooke, J.P. Chilton, D.J. Fray, Mass transfer kinetics of the ferrous-ferric electrode process in copper sulphate electrowinning electrolytes, Trans. Instn. Min. Metall. (Sec. C: Mineral Processing Extr. Metall.) 98 (1989) 123–131.
[10] S.P. Sandoval, W.J. Dolinar, J.W. Langhans, K.P.V. Lei, A substitute anode reaction for the electrowinning of copper, in: W.C. Cooper (Ed.), Proceedings of the COPPER '95 International Conf, vol. 3, The Metallurgical Society of CIM, Toronto, Canada, 1995, pp. 423–435.
[11] L. Cifuentes, R. Glasner, G. Crisóstomo, J.M. Casas, Thermodynamics and kinetics of a copper electrowinning cell based on reactive electrodialysis, in: J.E. Dutrizac, C.G. Clement (Eds.), Proceedings of the Copper 2003 International Conference, Santiago, Chile, November 30th – December 3rd, 2003, Copper Electrorefining and Electrowinning, vol. V, Canadian Institute of Mining, Metallurgy and Petroleum, 2003, pp. 623–637.
[12] L. Cifuentes, R. Glasner, J.M. Casas, Aspects of the development of a copper electrowinning cell based on reactive electrodialysis, Chem. Eng. Sci. 59 (2004) 1087–1101.
[13] J.M. Casas, F. Alvarez, L. Cifuentes, Aqueous speciation of sulfuric acid–cupric sulphate solutions, Chem. Eng. Sci. 55 (2000) 6223–6234.
[14] J.M. Casas, J.P. Etchart, L. Cifuentes, Aqueous speciation of arsenic in sulfuric acid and cupric sulfate solutions, AIChE J. 49 (8) (2003) 2199–2210.
[15] J.M. Casas, G. Crisóstomo, L. Cifuentes, Aqueous speciation of the Fe(II)–Fe(III)–H_2SO_4 system at 25 and 50 °C, Hydrometallurgy 80 (2005) 254–264.
[16] J. Newman, Transport processes in electrolytic solutions, in: C.W. Tobias (Ed.), Advances in Electrochemistry and Electrochemical Engineering, New York, USA, 1967, pp. 87–135.
[17] F. Hine, Electrode Processes and Electrochemical engineering, Plenum Press, New York, USA, 1985.
[18] K. Scott, Electrochemical Reaction Engineering, Academic Press, London, England, 1991.
[19] B. Steffen, I. Rousar, Numerical methods for electrochemical modelling—I, Electrochim. Acta 40 (1995) 379–386.
[20] H. Aminian, C. Bazin, D. Hodouin, C. Jacob, Simulation of SX-EW pilot plant, Hydrometallurgy 56 (2000) 13–31.
[21] L. Cifuentes, G. Crisóstomo, J.P. Ibáñez, J.M. Casas, F. Alvarez, G. Cifuentes, On the electrodialysis of aqueous H_2SO_4–$CuSO_4$ electrolytes with metallic impurities, J. Membr. Sci. 207 (2002) 1–16.
[22] J.O'M. Bockris, A.K.N. ReddyModern Electrochemistry, vol. 2A, Plenum Press, New York, USA, 2000.
[23] C. Gavach et al., Influence of cations on the proton leakage through anion exchange membranes, J. Membr. Sci. 110 (1996) 181–190.
[24] G. Pourcelly, Y. Lorrain, C. Gavach, Transport mechanism of sulfuric acid through an anion exchange membrane, Desalination 109 (1997) 231–239.
[25] J.M. Casas, G. Crisóstomo, L. Cifuentes, Aqueous speciation of electrowinning solutions, in: P.A. Riveros, D. Dixon, B. Dreisinger, J. Menacho (Eds.), Proceedings of Copper 2003, International Conference, Santiago, Chile, November 30–December 3, 2003, Hydrometallurgy of Copper, Book 1, vol. VI, Canadian Institute of Mining, Metallurgy and Petroleum, 2003, pp. 441–456.
[26] D.B. Spalding, Mathematical Modelling of Fluid Mechanics, Heat Transfer and Chemical Reaction Processes, CFDU, Imperial College, London, England, 1980.